advances in Technology

Adv. Technol. ***2021***, *1(1), 127-146*

Research Paper

Dynamic Optimization Self-adaptive AI Controller for a Four-wheel Independent Drive Electric Rover

H. R. Jayetileke,[a,*] W. R. de Mel,[b] and H. U. W. Ratnayake[c]

[a] Department of Mechanical Engineering, The Open University of Sri Lanka, PO Box 21, Nawala, Nugegoda 10250, Sri Lanka

[b] Department of Materials and Mechanical Technology, University of Sri Jayewardenepura, Homagama 10200, Sri Lanka

[c] Department of Electrical and Computer Engineering, The Open University of Sri Lanka, PO Box 21, Nawala, Nugegoda 10250, Sri Lanka

Email correspondence: hasithajayetileke@gmail.com, hrjay@ou.ac.lk (H.R. Jayetileke)

Received: 29 March 2021; Revised: 28 April 2021; Accepted: 5 May 2021; Published: 31 May 2021

Abstract

In this paper, a dynamic optimization self-adaptive controller for a four-wheel independent drive electric rover has been investigated to enhance the dynamic stability. The proposed self-adaptive AI controller is based on dynamic Fuzzy Logic (FL) control mechanism. The dynamic self-adaptive properties have been integrated into the proposed FL controller through a dynamically tuned Particle Swarm Optimization (PSO) mechanism. Nevertheless, the dynamic FL controller and the dynamic PSO mechanism has been synchronized together for every sampling instance *k* to obtain the optimum performance of the electric rover. In this electric rover, all the four wheels have a fixed orientation and each wheel powered by a 250-Watt Brushless Direct Current (BLDC) motor through separate gear ratio mechanisms to obtain the desired torque and angular velocity. Therefore, the steering mechanism was achieved in this rover through the proposed AI controller, which was based on the differential speed mechanism. However, this paper presents the control methodology and obtained test results related to straight road tests under different slippery road conditions. The rover test results show that on different slippery road conditions the proposed PSO based FL controller has maintained the wheel slip ratio of all the four wheels which was less than 0.35 approximately. Here, the translational speed has been limited to 40 km/hr approximately within its recorded top speed of 90 km/hr while maintaining the desired fix orientation.

Keywords: Artificial intelligence, fuzzy logic, particle swarm optimization, brushless direct current motor, four-wheel independent drive

https://doi.org/10.31357/ait.v1i1.4873

Introduction

The concept of a self-adaptive AI Controller is examined in this paper to enhance the rover (vehicle) stability during its fastest acceleration and deceleration. It not only dramatically reduces the chances of an accident, but also enhances the performance of the vehicle because intelligent control methods attempt to emulate important characteristics of human intelligence [1]. The basic idea behind the need of a self-adaptive AI (Traction control system) is due to the difference between traction of different wheels showing apparent losses (energy losses) of road grip that compromise steering control and stability of vehicles [2]. In a four-wheel-drive vehicle, for example, certain circumstances may arise where the surface traction or friction of all the wheels differs from one another; however, the power is the same for every wheel on each contacted surface. In such a case, if the vehicle speed is less than the wheel speed (vehicle speed < wheel speed) of a specific wheel, that wheel will slip.

Moreover, the difference in slip may occur due to vehicle being turned or because of different road conditions for different wheels [3]. When a vehicle is traveling at high speeds and turns, its outer and inner wheels rotate at various speeds, which must be controlled by a controller to achieve a desired turning radius without losing its stability. It is demonstrated that even in such cases, wheels can slip due to various of traction conditions which gives rise to non-linear behaviour [4].

Therefore, based on previous works & approaches to research problem in similar nature, the technical methodology is concerned with the development of fuzzy logic controller with self-optimization mechanism (Particle Swarm Optimization (PSO)) of its tuning parameters until desired level of performance is obtained.

Rufei Hou et. el., [5] have developed a hierarchical steering stability control strategy for a Four Hub-Motor Independent-Drive Electric Vehicle (4MIDEV) on a road with varying adhesion coefficient. Chentong Bian et. al., [6] have approached this research problem by

considering the longitudinal dynamic characteristics that takes place in the four-wheel drive electric vehicle. Valentin Ivanov et. al., [7] describe approaches to enhance the vehicle stability incorporating the transient road friction by regulating the wheel slip separately on each wheel. Yong Chen et. al., [8] have developed a lateral stability controller, an in-vehicle motion controller, which yields the generalized force and generalized yaw moment required of the vehicle, in two modes. Moreover, which mode to be activated is determined by stability judgment controller, based on phase portraits of sideslip angle and yaw rate. Bogdan Gilev, [9] has developed a vehicle traction system which is based on Neural Predictive control mechanism. A. A. Ahmed and A. F. Alshandoli, [10] describe approaches to solve this problem by implementing lateral stability and vehicle handling mechanism based on a 14-DOF full vehicle model and using two control methods. One is fuzzy PID control theory and the other is a neural network controller. Nguyen Huy Hung et. el., [11] have designed and developed a simulation based Kinematic Model Reference Adaptive Controller for a Lurking Type Automated Guided Vehicle using Traction Drive Unit. To control the non-linear behaviour of the automated guided vehicle, the developed kinematic model is based on non-linear Lyapunov stability theory. Amornwongpeeti et. el., [12] have made the approached this research problem by developing an adaptive torque controller based on Model Reference Adaptive Control technique for Interior Permanent Magnet Synchronous Motor drive systems for electric vehicles.

According to today's context, most of these vehicle adaptive traction controllers are model-reference controllers. Therefore, the non-linear relationship between the input and output parameters of the plant (vehicle model) needs to model based on sophisticated mathematical models [13]. Therefore, to overcome the drawbacks in adaptive model-reference control mechanisms, the proposed controller is based on an adaptive AI control mechanism. In that case, compared to traditional adaptive control strategies, the novelty of the proposed AI control

mechanism is its ability of controlling the non-linear behaviour of the rover without following a sophisticated mathematical reference- model while adapting its tuning parameters [14]. These parameters of the AI controller are adapted according to a developed self-optimization mechanism (PSO), which was dynamically tuned through another separately dedicated AI (Takagi-Sugeno-Kang (TSK) FL) controller [14]. Nevertheless, to obtain the optimum controlled output the proposed PSO based AI controller and the TSK-FL controller have synchronized for every sample instance k.

The current study describes the mechanical dynamics that take place in the vehicle model, differential fuzzy logic controller with dynamically optimized fuzzy inference mechanism through PSO model designed, straight road tests carried out on slippery road conditions to analyze performance of the AI controller designed and conclusions.

Mechanical Dynamics of the Four-Wheel Drive Electric Rover (4-WD ER)

To analyze and control the dynamic behaviour of the rover through the proposed AI controller, mathematical models have been developed. Based on these mathematical models the input information (for the controller) such as the wheel slip ratio and the ground-tire surface friction coefficient have been obtained while considering the acting dynamic forces (calculated based on the measured orthogonal accelerations through the accelerometer) into the directions of longitudinal force, lateral force and the radial force. Moreover, to enhance the dynamic stability of the rover pitch motion, yaw motion and the roll motion have been measured through the installed gyroscope. Therefore, to optimize the wheel slip ratio of the rover to enhance the stability during its fastest acceleration and deceleration the system model for orthogonal forces, tire model for wheel slip and tire model for ground-tire surface friction coefficient have been identified.

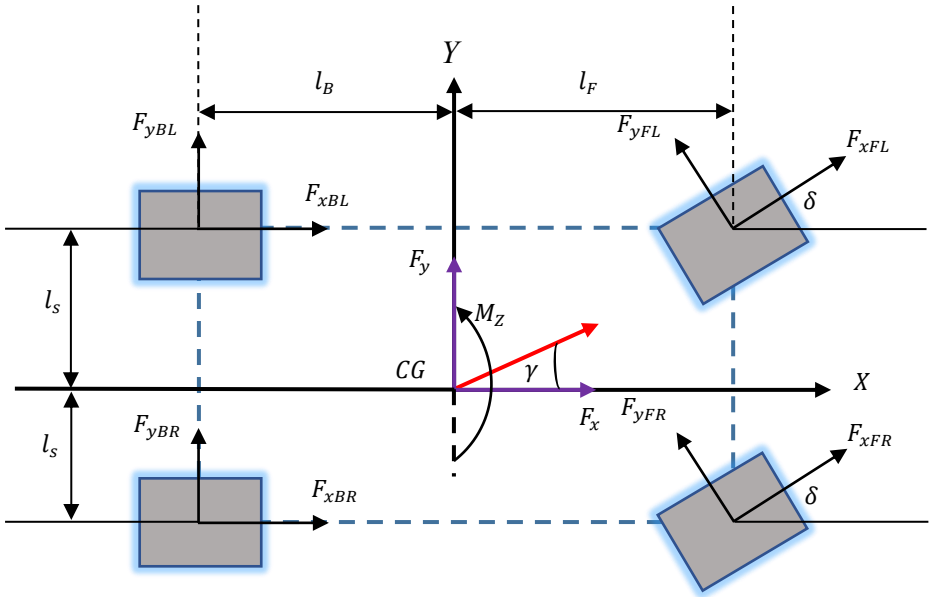

Figure 1. Schematic of the rover model

Rover System Model

As discussed by Alipour H. et al., [15] it shows that the mathematical model which was derived for a four-wheel independent vehicle to enhance the stability by considering the lateral forces, longitudinal forces, and the yaw motion. As shown in Figure 1, the simplified dynamic equation adapted for this developed rover could be expressed as Equation 1. However, the dynamic model of the rover for a steering angle δ could be expressed as equation A1.

V_x is the longitudinal velocity of the rover, V_y the lateral velocity of the rover, γ the yaw rate of the rover, M the mass of the rover, F_{xj} the longitudinal forces of each tire, F_{yj} the lateral forces of each tire. Here j would be FL, FR, BL and BR.

$$\begin{cases} M\dot{V}_x = (F_{xFL} + F_{xFR}) + F_{xBL} + F_{xBR} + MV_y\gamma \\ M\dot{V}_y = \left(F_{yFL} + F_{yFR}\right) + F_{yBL} + F_{yBR} - MV_x\gamma \\ I_z\dot{\gamma} = (F_{xFR} - F_{xFL} + F_{xBR} - F_{xBL})l_s - \left(F_{yFR} + F_{yBR}\right)l_r + (F_{xFR} + F_{xFL})l_f \end{cases}$$

(Equation 1)

Equation 1 could represent in state-space form as Equation 2:

$$\begin{bmatrix} V_x \\ V_y \\ V_z \end{bmatrix} = \begin{bmatrix} V_y\gamma \\ -V_x\gamma \\ 0 \end{bmatrix} + B_y \begin{bmatrix} F_{yFL} \\ F_{yFR} \\ F_{yBL} \\ F_{yBR} \end{bmatrix} + B_x \begin{bmatrix} F_{xFL} \\ F_{xFR} \\ F_{x_{BL}} \\ F_{x_{BR}} \end{bmatrix} \quad \text{(Equation 2)}$$

where B_x and B_y could be expressed as Equation A2.

However, in the developed model, all the four-wheels has a fixed orientation. Therefore, the steering angle δ is zero. In that case according to Equation A2, B_x and B_y could be simplified as follows:

$$B_x = \begin{bmatrix} \frac{1}{M} & \frac{1}{M} & \frac{1}{M} & \frac{1}{M} \\ 0 & 0 & 0 & 0 \\ \frac{-l_s}{I_z} & \frac{l_s}{I_z} & \frac{-I_s}{I_z} & \frac{I_s}{I_z} \end{bmatrix};\ B_y = \begin{bmatrix} 0 & 0 & 0 & 0 \\ \frac{1}{M} & \frac{1}{M} & \frac{1}{M} & \frac{1}{M} \\ \frac{l_F}{I_z} & \frac{l_F}{I_z} & \frac{-I_r}{I_z} & \frac{I_r}{I_z} \end{bmatrix} \because (\sin\delta = \sin 0 = 0) \text{ and } (\cos\delta = \cos 0 = 1)$$

As shown in Equation 2, to compute all the variables V_x, V_y, $\dot{\gamma}$ and γ the real-time measured data through the accelerometer-gyro module was considered. The rover inertia I_z was approximately calculated by considering the rover as a solid cuboid and the aerodynamic drag force F_D was neglected due its small-scale (as described in appendix A, justified based on the observed test results). Therefore, as shown in Figure 1, all the F_{xj} and F_{yj} (lateral and longitudinal) forces are computed according to Equation 2.

Tire Model to Identify the Wheel-Slip (S_j)

In high-speed and low-speed conditions, longitudinal wheel slip of each wheel needs to be regulated because the tire travelled distance is different from the expected distance from its peripheral speed [15]. This non-linear behaviour could be analyzed considering the behaviour of S_j, where S_j is defined as the relative difference between tire peripheral speed and tire center speed (or the rover translational speed) as expressed in Equation 3:

$$S_j = \frac{\omega_j R_{eff} - V_{xj}}{\max\left(V_{xj}, \omega_j R_{eff}\right)}; \qquad \begin{matrix} R_{eff}\omega_j < V_x & \text{for deceleration} \\ > V_x & \text{for acceleration} \end{matrix} \qquad \text{(Equation 3)}$$

where $j = FL, FR, BL$ and BR. Here R_{eff} is the effective tire radius, ω_j the angular speed of the j-th tire, V_x the longitudinal speed at the center of the j-th wheel. Therefore, Equation 3 shows that, when $R_{eff}\omega_j > V_x$ a positive wheel-slip ($S_j > 0$) indicates that the wheels are spinning and when $R_{eff}\omega_j < V_x$ a negative wheel-slip ($S_j < 0$) indicates that the wheels are skidding. This causes the lateral slip in rover. To analyze S_j during the fastest acceleration and deceleration the friction coefficient μ_j need to be identified. Therefore, a tire model has been considered by considering the friction force $F_{(friction)_j}$.

Tire Model to Identify the Kinetic Friction-Coefficient (μ_j)

As shown in Figure 2, when the tire is spinning around its axel if the friction force $F_{(friction)_j}$ between the tire and the road surface is good enough, then the rover moves forward. If the resultant $F_{(friction)_j}$ is not good enough, then the wheel will spin around its axel. This could be expressed as Equation 4:

$$T_{(Drive-shaft)_j} > \left\{T_{(friction)_j} = F_{(friction)_j} R\right\} \Longrightarrow Slip \qquad \text{(Equation 4)}$$

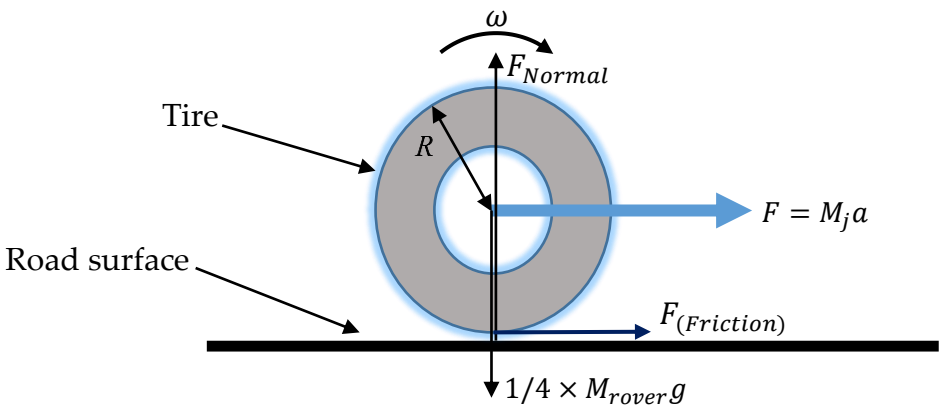

Figure 2. Acting forces on each tire of the rover

Therefore, all these four-wheels will be generated a resultant friction

force $F'_{(friction)}$ in the same direction. The $F'_{(friction)}$ could be expressed as Equation 5:

$$F'_{(friction)} = \sum_{j=FL}^{BR} F_{(friction)_j} = \mu_{(kinetic)Avg} M_{rover} g \qquad \text{(Equation 5)}$$

where: R is the radius of the tire, $\mu_{(kinetic)Avg}$ the average friction coefficient, $F_{Normal} = (M_{rover} g)$ the normal force, M_{rover} the total mass of the rover and g the gravitational acceleration. Therefore, according to Newton's 2nd law the maximum acceleration a_{Max} into the longitudinal direction could be expressed as Equation 6.

$$a_{Max} = \frac{F'_{(friction)}}{M_{rover}} \qquad \text{(Equation 6)}$$

Substituting Equation 5 into Equation 6 the kinetic friction coefficient $\mu_{(kinetic)Avg}$ of each surface could be expressed as Equation 7 (where $g \approx 9.8\ ms^{-2}$):

$$\mu_{(kinetic)Avg} = \frac{|a_{Max}|}{g} \Longrightarrow \frac{1}{9.8}\ |a_{Max}| \qquad \text{(Equation 7)}$$

Design and Development of the Dynamic Optimization Self-Adaptive AI Controller of the Rover

The proposed AI controller is a combination of three main controllers. These are the "Steering FLC" (S-FLC), "Differential FLC" (D-FLC) and the "Dynamic PSO-FLC". However, this paper analyses the performance of the rover on slippery straight road conditions instead of slippery curve road conditions. Therefore, the development of D-FLC which was dynamically optimized through the PSO-FLC has been discussed. The developed PSO-FLC [14] is based on 49 static fuzzy rules [16] and with an identified, dynamically fuzzy rules generating mechanism [17].

Design and Development of the Differential FLC (D-FLC)

Figure 3 shows, the main structure of the D-FLC. Figure 4 to Figure 9 shows, the proposed D-FLC, consists of six fuzzy input variables and

four fuzzy output variables with all the related membership functions of linguistic variables.

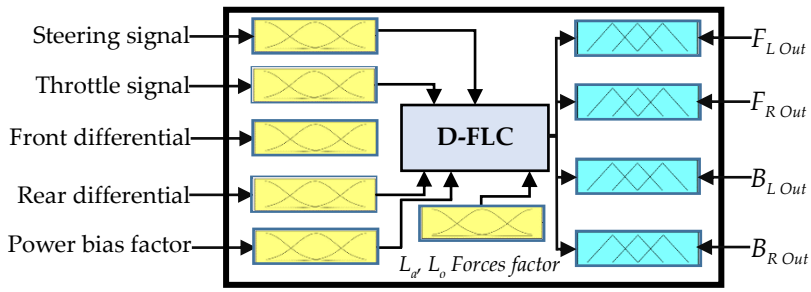

Figure 3. The block diagram representation of the Differential FLC (D-FLC)

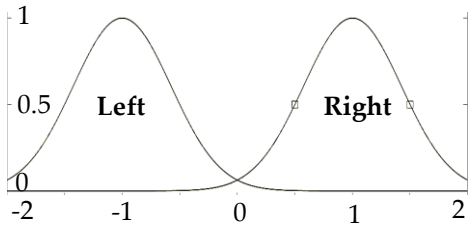

Figure 4. Membership functions of the input fuzzy variable "Steering signal"

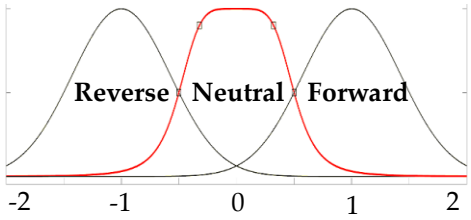

Figure 5. Membership functions of the input fuzzy variable "Throttle signal"

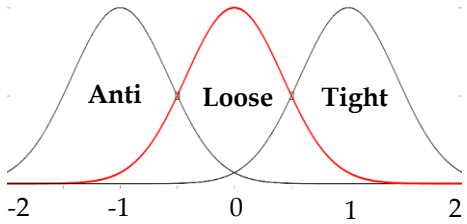

Figure 6. Membership functions of the input fuzzy variable "Front differential"/ "Rear differential"

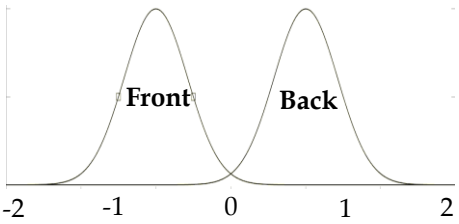

Figure 7. Membership functions of the input fuzzy variable "Power bias factor"

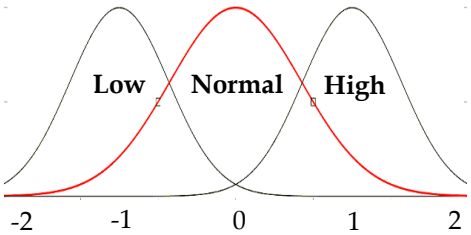

Figure 8. Membership functions of the input fuzzy variable "Lateral and longitudinal force factor"

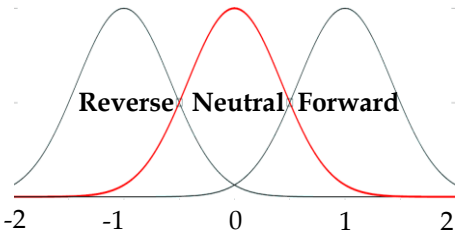

Figure 9. Membership functions of output fuzzy variable "$F_{L\,Out}$, $F_{R\,Out}$, $B_{L\,Out}$ and $B_{R\,Out}$"

Design and Development of a Fuzzy Rule-Base for the Differential FLC (D-FLC)

Table B1 shows the developed seventeen fuzzy rules-based for D-FLC. These fuzzy rules show the relationship between the fuzzy inputs and fuzzy outputs, with "if", "and" and "then" conditions. For example, the 3rd fuzzy rule could be read through Table B1, as follows:

3rd Fuzzy Rule:

If T_r is "**Neutral**" ***then*** the {$F_{L\,Out}$ is "**Neutral**", and $F_{R\,Out}$ is "**Neutral**" and $B_{L\,Out}$ is "**Neutral**" and $B_{R\,Out}$ is "**Neutral**"}. Where T_r is the "Throttle signal" and P_b is the "Power bias factor".

Analysis of the Observed Test Results

To analyze the performance of the developed AI controller with all types of road constraints, straight, slope, descent and curved roads have been taken into account during the fastest acceleration and deceleration. However, this paper is focused on the road tests that have taken placed on straight roads under different traction conditions.

The Electric Rover (ER) Straight-Road Test

The straight road test was performed on a slippery wet grass surface. When the rover moves on a straight road (trajectory) even under different traction conditions (different friction coefficients μ_j) the orientation of the rover should be the same over time as its desired orientation. Therefore, to maintain a particular desired orientation based on the observed data through the installed gyroscope, the developed AI controller should synchronize all the angular velocities (r.p.m.) of each wheel to maintain the desired orientation (fixed orientation) (because the developed rover turns based on differential speed technique has not been discussed in this paper).

Figure 10 shows the desired throttle signal and the desired steering angle which represents a zero-degree yaw angle (in its neutral position) over the operation time-period of the straight road test (fed wirelessly

based on IEEE 802.15.04 protocol through a computer-controlled joystick).

As shown in Figure 11, the μ_j variations over time, which is computed according to Equation 7, which is less than 0.4 and the average μ_j is around 0.12. This indicates that the wet grass road surface is highly slippery. Therefore, within all these conditions optimizing the wheel slip of each wheel and maintaining a desired particular yaw angle, over the operation time-period, which was highly sophisticated.

Figure 12 shows, the r.p.m. of each wheel respect to the average desired r.p.m *refWs*. For the peak edge of the r.p.m. of each independent wheel, the steady-state error E_{ss} and the steady state error as a percentage E_{ss}% could be as expressed according to Table 1. At this peak r.p.m. point the maximum average r.p.m. and the translational velocity of the rover is 1024.4 r.p.m. and 25.09 km/hr. respectively.

Table 1. Steady state error percentage (E_{ss}%) of each independent wheel

Wheel of the rover	**Steady sate error (E_{ss}) (r.p.m.)**	**Steady sate error % (E_{ss}%) (r.p.m.)**
Front-Left (FL)	58.16	5.24
Front-Right (FR)	68.81	6.27
Back-Left (BL)	-28.65	-2.95
Back-Right (BR)	-51.82	-5.36

Figure 13 and Figure 14 shows the three orthogonal accelerations ("*AccX*: longitudinal", "*AccY*: lateral" and "*AccZ*: radial") and the three gyro-angles ("*GyYaw*: Yaw", "*GyPit*: Pitch" and "*GyRol*: Roll") that have been observed, when observing the wheel speed data.

Moreover, Figure 13 shows that when the rover reached a peak r.p.m., then the radial acceleration has rapidly fluctuated. This was taken place due to an uneven road surface.

Figure 14 shows that, the rover has come across a slop about 30^0 within around 3.5 seconds. Again, around for 3.5 seconds, the rover actual yaw

angle has been moved away around 10^0 from its desired yaw angle. Compared to its total travel distance (recorded distance is 105.64 m) the yaw angle variation is 10^0 respect to the initial position. Moreover, around 2^0 of roll angle has taken place due to the slope of the grass surface into the lateral direction of the rover.

Based on the observed wheel speed data the wheel slip ratio, S_j was calculated according to Equation 3 in real-time operation for different road surfaces (for different friction coefficients). Figure 15 shows that, the proposed PSO-FLC mechanism has enhanced the performance of the rover by synchronizing all the four-wheel speeds within an optimum amount. As shown in Figure 15, the "*mWsrFL*", "*mWsrFR*", "*mWsrBL*" and "*mWsrBR*" represent the measured wheel slip ratio of the front-left wheel, front-right wheel, back-left wheel and the back-right wheel. As shown in Figure 15, it could be identified that all the wheel slip ratio graphs have the same shape. These phenomena have been taken place because the straight road test was performed on an approximately even kinetic friction coefficient surface. Moreover, it shows that, the wheel slip ratio of all the wheels is positive and the proposed PSO-FLC has maintained the wheel slip ratio of all the wheels within a range less than 0.35.

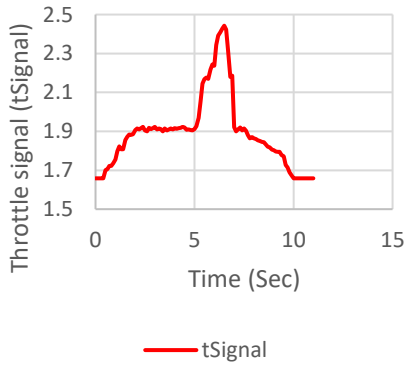

Figure 10. The throttle signal which is given to the controller to achieve the desired translational velocity/ The neutral position of the steering angle-level is 1.7 (to achieve a zero-yaw angle)

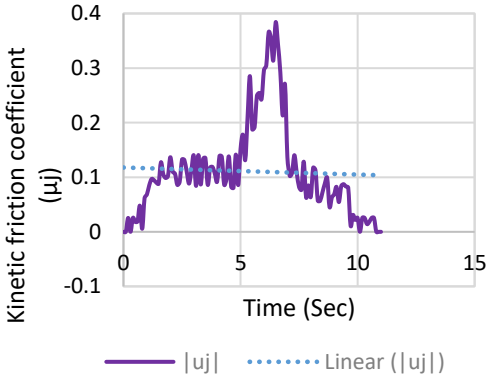

Figure 11. The variation of the kinetic friction coefficient (μ_j) vs. time (Sec)

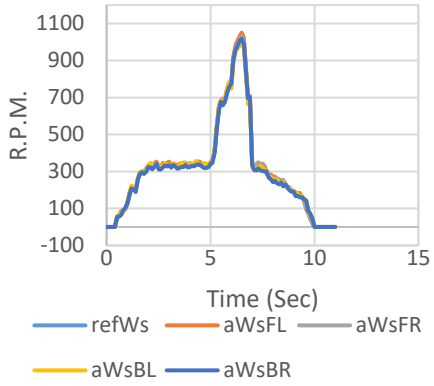

Figure 12. The reference r.p.m. (refWs) and the actual r.p.m. of each individual wheel vs. time

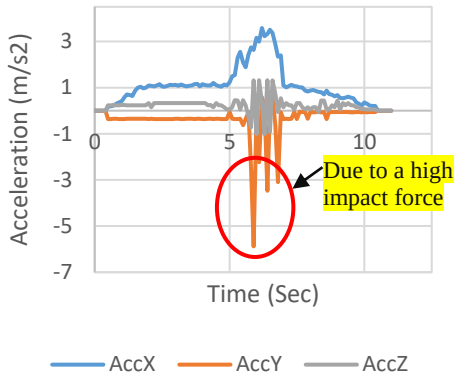

Figure 13. The actual three orthogonal accelerations vs. time of the rover

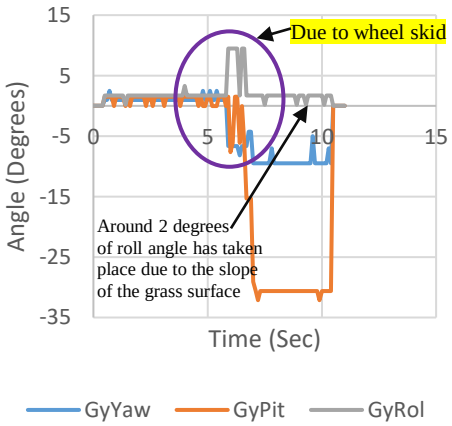

Figure 14. The actual Yaw angle, Pitch angle and the Roll angle vs. time of the rover

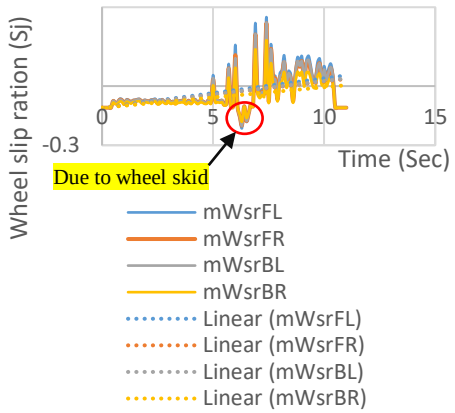

Figure 15. The wheel slip ratio (S_i) vs. time (Sec) of all the four-wheels

Conclusion

As discussed in the introduction, compared to previous work and approaches to the research problem in similar nature, the proposed fuzzy logic controller with self-optimization mechanism (PSO-FLC) has the capabilities to enhance the rover stability during its fastest acceleration, deceleration on slippery road conditions. The proposed AI controller with the design and developed D-FLC has the capabilities to drive the rover within a noticeable top speed of 90 km/hr. However, under test conditions (on slippery road conditions), the rover

translational speed drops up to 45 km/hr. Moreover, the proposed PSO-FLC with the D-FLC has maintained the wheel slip ratio of all the four wheels within an admirable amount which were less than 0.35 approximately on wet grass surface within an average friction coefficient μ_j of 0.12.

Conflict of Interest

The authors declare no conflict of interest.

References

[1] K. Chang, K. Chu, Y. Lin, J. Pan. Overview of Some Intelligent Control Structures and Dedicated Algorithms. In Automation and Control. IntechOpen. **2020**.

[2] Z. Li, P. Wang, H. Chen. Coordinated longitudinal and lateral vehicle stability control based on the combined-slip tire model in the MPC framework. Chinese Control and Decision Conference (CCDC). IEEE. **2020**, 103-105.

[3] N. Ghobadi, Narges, S. F. Dehkordi. Dynamic modeling and sliding mode control of a wheeled mobile robot assuming lateral and longitudinal slip of wheels. 7th International Conference on Robotics and Mechatronics (ICRoM). IEEE. **2019**, 150-155.

[4] S. Yamazaki, T. Fujikawa, and I. Yamaguchi. A study on braking and driving properties of automotive tires. Transactions of the Society of Automotive Engineers of Japan. **1992**, 23, 97-102.

[5] R. Hou, L. Zhai, T. Sun. Steering stability control for a four hub-motor independent-drive electric vehicle with varying adhesion coefficient. Energies. **2018**, 11, 2438.

[6] C. Bian, G. Yin, N. Zhang, L. Xu. Takagi-sugeno fuzzy model predictive controller design for combining lane keeping and speed tracking of four wheels steering and four wheels drive electric vehicle. 29th Chinese Control and Decision Conference (CCDC). IEEE. **2017**, 4067-4072.

[7] V. Ivanov, D. Savitski, K. Augsburg, P. Barber. Electric vehicles with individually controlled on-board motors: Revisiting the ABS design. International Conference on Mechatronics (ICM). IEEE. **2015**, 323-328.

[8] Y. Chen, S. Chen, Y. Zhao, Z. Gao, C. Li. Optimized handling stability control strategy for a four in-wheel motor independent-drive electric vehicle. IEEE. **2019**, 7, 17017-17032.

[9] B. Gilev, Modeling the Vehicle Traction System and Developed Neural Predictive Controller. International Conference on High Technology for Sustainable Development (HiTech). IEEE. **2018**, 1-4.

[10] A. A. Ahmed, A. F. S. Alshandoli. Using of Neural Network Controller and Fuzzy PID Control to Improve Electric Vehicle Stability Based on A14-DOF

Model. International Conference on Electrical Engineering (ICEE). IEEE. **2020**, 1-6.

[11] H. H. Nguyen, T. T. Nguyen, T. T. Nguyen, H. L. Phan. Kinematic Model Reference Adaptive Controller for a Lurking Type Automated Guided Vehicle using Traction Drive Unit. International Conference on Advanced Mechatronic Systems (ICAMechS). IEEE. **2020**, 108-112.

[12] S. Amornwongpeeti, O. Kiselychnyk, J. Wang, N. Shatti, N. Shah, M. Soumelidis. Adaptive torque control of IPMSM motor drives for electric vehicles. 26th International Symposium on Industrial Electronics (ISIE). IEEE. **2017**, 226-231.

[13] A. Shekhar, A. Sharma. Review of model reference adaptive control. International Conference on Information, Communication, Engineering and Technology (ICICET). IEEE. **2018,** 1-5.

[14] H. R. Jayetileke, W. R. de Mel, H. U. W. Ratnayake. A Dynamic AI Controller, for a Field-Oriented Controlled BLDC Motor to Achieve the Desired Angular Velocity and Torque. International Journal of Intelligent Systems and Applications in Engineering. IJISAE. **2019**, 7, 166-182.

[15] H. Alipour, M. Sabahi, M. B. B. Sharifian. Lateral stabilization of a four-wheel independent drive electric vehicle on slippery roads. Mechatronics. **2015**, 30, 275-285.

[16] H. R. Jayetileke, W. R. de Mei, H. U. W. Ratnayake. Real-time fuzzy logic speed tracking controller for a DC motor using Arduino Due. International Conference on Information and Automation for Sustainability. IEEE. **2014**, 1-6.

[17] H. R. Jayetileke, W. R. de Mel, H. U. W. Ratnayake. Modelling and simulation analysis of the genetic-fuzzy controller for speed regulation of a sensored BLDC motor using MATLAB/SIMULINK. International Conference on Industrial and Information Systems (ICIIS). IEEE. **2017**, 1-6.

Appendix - A

As shown in Figure 1 when the steering angle δ take place the complete dynamic model could be expressed as Equation A1.

$$\begin{cases} M\dot{V}_x = (F_{xFL} + F_{xFR})\cos\delta - \left(F_{yFL} + F_{yFR}\right)\sin\delta + F_{xBL} + F_{xBR} - F_D + MV_y\gamma \\ M\dot{V}_y = \left(F_{yFL} + F_{yFR}\right)\cos\delta + (F_{xFL} + F_{xFR})\sin\delta + F_{yBL} + F_{yBR} - MV_x\gamma \\ I_z\dot{\gamma} = \left(F_{yFL}\sin\delta - F_{xFL}\cos\delta + F_{xFR}\cos\delta - F_{yFR}\sin\delta\right)l_s + (F_{xBR} - F_{xBL})l_s \\ \qquad -\left(F_{yFR} + F_{yBR}\right)l_r + \left((F_{xFR} + F_{xFL})\cos\delta + (F_{xFR} + F_{xFL})\sin\delta\right)l_f \end{cases}$$

(Equation A1)

where $F_D = \frac{1}{2}\,\rho_a C_D A V_x^2$ is the aerodynamic drag force, ρ_a the air density, C_D the aerodynamic drag coefficient and A the front area of the rover. Compared to the longitudinal forces, the rover aerodynamic drag force F_D is negligible ($F_D \approx 0$) due to the small front area of the rover and during the straight road tests as described in the section test results analysis, the translational speed of the rover is around 40 km/hr.

Figure 12, Figure 13 and Table 1 shows that, with this speed limit the aerodynamic drag force is small compared to its effect on the rover translational velocity into the longitudinal direction (As shown in Figure 12, except the peak point the steady state error percentage E_{ss}% of the r.p.m. of each wheel is less than 4%).

Therefore, when $F_D = 0$, Equation A1 could be expressed in state-space form as Equation 2. In Equation 2 where B_x and B_y could be expressed as Equation A2.

$$B_x = \begin{bmatrix} \frac{\cos\delta}{M} & \frac{\cos\delta}{M} & \frac{1}{M} & \frac{1}{M} \\ \frac{\sin\delta}{M} & \frac{\sin\delta}{M} & 0 & 0 \\ \frac{l_F \sin\delta - l_S \cos\delta}{I_z} & \frac{l_F \sin\delta + l_S \cos\delta}{I_z} & \frac{-I_S}{I_z} & \frac{I_S}{I_z} \end{bmatrix};$$

$$B_y = \begin{bmatrix} \frac{-\sin\delta}{M} & \frac{-\sin\delta}{M} & 0 & 0 \\ \frac{\cos\delta}{M} & \frac{\cos\delta}{M} & \frac{1}{M} & \frac{1}{M} \\ \frac{l_F \cos\delta + l_S \sin\delta}{I_z} & \frac{l_F \cos\delta - l_S \sin\delta}{I_z} & \frac{-I_r}{I_z} & \frac{I_r}{I_z} \end{bmatrix}$$

(Equation A2)

Moreover, the steering radius of the developed rover maintained through differential speed mechanism (have not described in this paper). Therefore, all the wheels of the rover have a fixed orientation where the front wheel steering angle takes place zero degrees ($\delta = 0$).

Appendix - B

Table B1. The fuzzy rule-base for the D-FLC

	Fuzzy inputs				**Fuzzy outputs**			
No.	***if***	***and***	***and***	***and***	***then***			
1.	P_b is Front	-	-	-	$B_{L\,Out}$ is Neutral	$B_{R\,Out}$ is Neutral	-	-
2.	P_b is Back	-	-	-	$F_{L\,Out}$ is Neutral	$F_{R\,Out}$ is Neutral	-	-
3.	T_r is Neutral	-	-	-	$F_{L\,Out}$ is Neutral	$F_{R\,Out}$ is Neutral	$B_{L\,Out}$ is Neutral	$B_{R\,Out}$ is Neutral
4.	T_r is Reverse	-	-	-	$F_{L\,Out}$ is Reverse	$F_{R\,Out}$ is Revers	$B_{L\,Out}$ is Revers	$B_{R\,Out}$ is Revers
5.	S_s is Left	T_r is Forward	R_d is Loose	-	$B_{L\,Out}$ is Neutral	$B_{R\,Out}$ is Forward	-	-
6.	S_s is Right	T_r is Forward	R_d is Loose	-	$B_{L\,Out}$ is Forward	$B_{R\,Out}$ is Neutral	-	-
7.	S_s is Left	T_r is Forward	F_d is Loose	-	$F_{L\,Out}$ is Neutral	$F_{R\,Out}$ is Forward	-	-
8.	S_s is Right	T_r is Forward	F_d is Loose	-	$F_{L\,Out}$ is Forward	$F_{R\,Out}$ is Neutral	-	-
9.	T_r is Forward	-	-	-	$F_{L\,Out}$ is Forward	$F_{R\,Out}$ is Forward	$B_{L\,Out}$ is Forward	$B_{R\,Out}$ is Forward
10.	S_s is Left	T_r is Forward	R_d is Loose	L_f is High	$B_{L\,Out}$ is Neutral	$B_{R\,Out}$ is Neutral	-	-
11.	S_s is Right	T_r is Forward	R_d is Loose	L_f is High	$B_{L\,Out}$ is Neutral	$B_{R\,Out}$ is Neutral	-	-
12.	S_s is Left	T_r is Forward	F_d is Loose	L_f is High	$F_{L\,Out}$ is Neutral	$F_{R\,Out}$ is Neutral	-	-
13.	S_s is Right	T_r is Forward	F_d is Loose	L_f is High	$F_{L\,Out}$ is Neutral	$F_{R\,Out}$ is Neutral	-	-
14.	S_s is Left	T_r is Forward	R_d is Tight	L_f is High	$B_{L\,Out}$ is Forward	$B_{R\,Out}$ is Neutral	-	-
15.	S_s is Right	T_r is Forward	R_d is Tight	L_f is High	$B_{L\,Out}$ is Neutral	$B_{R\,Out}$ is Forward	-	-
16.	S_s is Left	T_r is Forward	F_d is Tight	L_f is High	$F_{L\,Out}$ is Forward	$F_{R\,Out}$ is Neutral	-	-
17.	S_s is Right	T_r is Forward	F_d is Tight	L_f is High	$F_{L\,Out}$ is Neutral	$F_{R\,Out}$ is Forward	-	-

Appendix – C

Figure C1. The straight road test on a slippery wet grass surface (captured when the speed of the rover is around 42.8 km/hr.)

Figure C2. Top recorded speed while running on a gravel soil surface (as shown in Figure C4 the top recorded speed is around 90 km/hr)

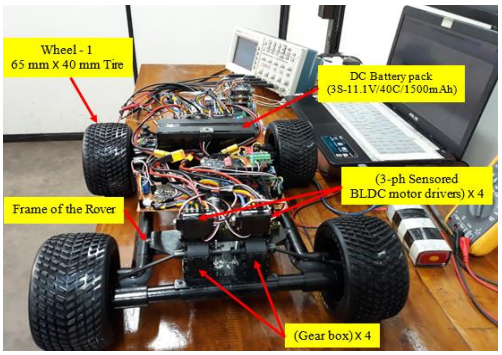

Figure C3. The front view of the Electric Rover

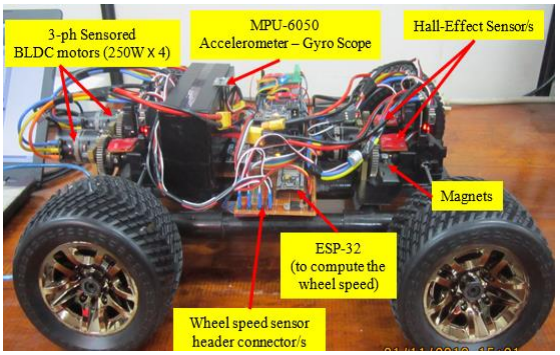

Figure C4. The side view of the Electric Rover

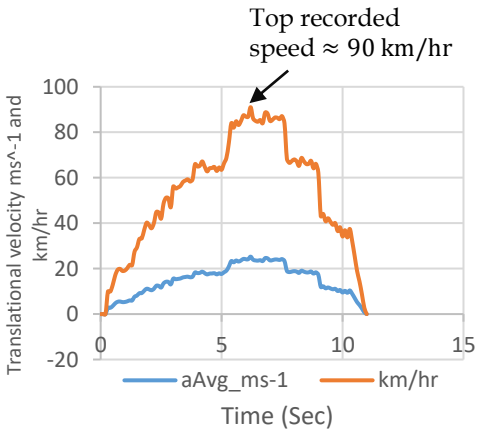

Figure C5. Top recorded speed of the rover (have not discussed in this paper)

Table C1: The physical parameters of the electric rover

Physical parameter	**Amount with units**
Rover Width (W)	0.415 m
Rover Height (H) (Ground clearance)	0.06 m
Rover Length (L)	0.465 m
Diameter of a wheel	0.13 m
Weight of the rover body (M_B)	3.288 kg
Weight of a wheel (M_{Wh})	0.064 kg
Total weight of the rover (M_R)	5.066 kg